Journal of Applied and Fundamental Sciences

STUDY OF NEUTRINOLESS DOUBLE-BETA DECAY AND JARLSKOG INVARIANT FOR THE TWO-ZERO TEXTURES IN MINIMAL EXTENDED SEESAW MECHANISM

Sangeeta Dey*, Priyanka Kumar
Department of Physics, Cotton University, Panbazar, Guwahati
*For correspondence. (sangeetarimpi39@gmail.com)

Abstract: In this work we study the effective Majorana mass $|m_{ee}|$ in neutrinoless double-beta decay for the two-zero textures of 4×4 neutrino mass matrices in minimal extended type-I seesaw (MES) mechanism i.e (3+1) scenario, incorporating one extra gauge singlet field S. The MES model deals with 3×3 (M_D),3×3 (M_R) and mass matrix 1×3 (M_S) which couples with the right-handed neutrinos and the singlet field S. Here only those two-zero textures are considered which are of rank 3, thereby the number of feasible zero textures reduces to 12, out of 15. In this work we consider the (4+4) scheme where the digits in the pair represent the number of zeros of M_D and M_R respectively, along with the one/two-zero textures of M_S. This formalism leads to one sterile neutrino in eV scale. We are motivated to work on eV scale sterile neutrino for the solution to the LSND anomaly which is still alive experimentally. We have also shown the $|m_{ee}|$ and J_{cp} plots for all the two-zero textures considered.

1. Introduction:

In the past decade a number of neutrino experiments have been performed which confirms that neutrinos are massive. Experiments performed in different parts of the globe has provided us with appreciable information on mixing angles (θ_{12},θ_{23},θ_{13}) and squared mass differences (Δm^2_{12},Δm^2_{13}) of three active neutrinos. Although precise and solid information have been provided by the experimentalists, the neutrino physics world is still filled with a number of anomalies which still strives for solutions. One such is the LSND anomaly [1], which detected an anomalous $\bar{\nu}_\mu - \bar{\nu}_e$ mode corresponding to a squared mass difference of eV^2 , which cannot be explained in the context of three neutrino paradigm. MiniBooNE experiment [2],Gallium Solar neutrino experiment [3, 4], reactor neutrino experiment [5] and cosmological observations also confirmed similar departures. All these anomalies hint towards the existence of an additional light sterile neutrino.

The basic Standard Model extensions include the existence of right-handed Majorana neutrino which is used to explain neutrino masses via type-I seesaw mechanism. There are a number of ways in which the Standard Model of particle physics can be extended to include the light sterile neutrinos [6, 7]. The minimal extension to the three neutrino scenario is the 3+1 scheme [8, 9] i.e three active neutrino and one sterile in the sub-eV and eV scale respectively.In (3+1)scheme , similar to the three neutrino scheme, a major role is played by seesaw mechanism for generating eV scale sterile neutrino mass by extending Type-I seesaw mechanism. This model is known as Minimal Extended (Type-I) Seesaw Mechanism (MES),where one singlet fermion 'S' is added along with three right-handed neutrinos.This results into a naturally occuring eV scale sterile neutrino without requiring to impose any tiny Yukawa term or mass scale.

Texture zeros of neutrino mass matrices in the three active neutrino paradigm has been studied extensively in the literature for mainly two reasons (1) reduction of number of free parameters of otherwise complicated textures of the mass matrices leading to enhance the predictivity of the models (2)the connection with the underlying flavor symmetry.In type-I seesaw mechanism, the zeros of the Dirac neutrino mass matrix M_D and Majorana mass matrix M_R propagate to zeros of the effective neutrino mass matrix M_ν. There are one/two/three/four possible zero textures in case of 4×4 neutrino mass matrices but three/four zero textures of $M_\nu^{4\times4}$ cannot be realised in MES framework because it requires M_D and M_R to be invertible, or they should not be singular. Here texture zeros of M_D and M_R under the (4+4)scheme has been considered,i.e 4 zeros of M_D and 4 zeros of M_R. Along with the zero textures of M_D and M_R, one/two-zero textures of the 1×3 mass matrix M_S , such that the desired

two-zero textures are realized in the $M_\nu^{4\times4}$ via MES mechanism. Since the determinant of 4×4 MES neutrino mass matrix vanishes, it must be a matrix of rank 3. Therefore atleast one of the active sterile neutrino has to be massless.There exist a total of 15 viable two zero textures out of which only 12 are of rank 3.

In this work we will study the dependence of effective electron neutrino mass $|m_{ee}|$ on the the Majorana CP phase α by considering constrained ranges of Majorana CP phases (α, β, γ) for all the considered two-zero textures studied in the paper [10]. We also calculate Jarlskog invariant J_{cp} of all the the two-zero textures considering constrained range of Dirac CP phases $(\delta_{13}, \delta_{14}, \delta_{24})$.

2. Two zero textures of $M_\nu^{4\times4}$:

I The considered two-zero textures of $M_\nu^{4\times4}$ of rank 3 is listed in Table 1. The zeros of $M_\nu^{4\times4}$ in MES results from the zeros of M_D, M_R and M_S. In predictive cases, there are a total of 8 zeros of M_D and M_R, therefore the number of possibilities we have are (4+4),(5+3) and (6+2) where the first number represent the number of zeros of M_D and the second of M_R. Here the (4+4) scheme is considered as it has maximum number of zeros in the right handed neutrino sector.

Table 1: Viable two-zero textures [11] of rank 3.Here X denotes the non-zero elements of the matrix.

A_1	A_2	B_3	B_4
$\begin{pmatrix}0&0&X&X\\0&X&X&X\\X&X&X&X\\X&X&X&X\end{pmatrix}$	$\begin{pmatrix}0&X&0&X\\X&X&X&X\\0&X&X&X\\X&X&X&X\end{pmatrix}$	$\begin{pmatrix}X&0&X&X\\0&0&X&X\\X&X&X&X\\X&X&X&X\end{pmatrix}$	$\begin{pmatrix}X&X&0&X\\X&X&X&X\\0&X&0&X\\X&X&X&X\end{pmatrix}$
C	D_1	D_2	E_1
$\begin{pmatrix}X&X&X&X\\X&0&X&X\\X&X&0&X\\X&X&X&X\end{pmatrix}$	$\begin{pmatrix}X&X&X&X\\X&0&0&X\\X&0&X&X\\X&X&X&X\end{pmatrix}$	$\begin{pmatrix}X&X&X&X\\X&X&0&X\\X&0&0&X\\X&X&X&X\end{pmatrix}$	$\begin{pmatrix}0&X&X&X\\X&0&X&X\\X&X&X&X\\X&X&X&X\end{pmatrix}$
E_2	F_1	F_2	F_3
$\begin{pmatrix}0&X&X&X\\X&X&X&X\\X&X&0&X\\X&X&X&X\end{pmatrix}$	$\begin{pmatrix}X&0&0&X\\0&X&X&X\\0&X&X&X\\X&X&X&X\end{pmatrix}$	$\begin{pmatrix}X&0&X&X\\0&X&0&X\\X&0&X&X\\X&X&X&X\end{pmatrix}$	$\begin{pmatrix}X&X&0&X\\X&X&0&X\\0&0&X&X\\X&X&X&X\end{pmatrix}$

3. Four zero textures of M_D:

The Dirac neutrino mass matrix M_D is a 3×3 non-symmetric matrix which has nine independent entries which takes the following form

$$M_D = \begin{pmatrix} a & b & c \\ d & e & f \\ g & h & i \end{pmatrix} \tag{1}$$

There are a total of ${}^9C_4$ i.e 126 possible four zero textures of M_D out of which 81 four zero textures are considered because of the requirement of nonsingular M_D.

4. Four zero textures of M_R:

There are 15 possible four zero textures out of which only 3 are non singular.

$$M_R^a = \begin{pmatrix} 0 & b & 0 \\ b & 0 & 0 \\ 0 & 0 & 0 \end{pmatrix}, M_R^b = \begin{pmatrix} 0 & 0 & C \\ 0 & D & 0 \\ C & 0 & 0 \end{pmatrix}, M_R^c = \begin{pmatrix} A & 0 & 0 \\ 0 & 0 & E \\ 0 & E & 0 \end{pmatrix} \tag{2}$$

5. Zero textures of M_S:

M_S is a 1×3 row matrix which couples the singlet field 'S' with the three right handed neutrinos. There can be one or two-zero textures of M_S. It was found that only one-zero textures of M_S lead to non-vanishing entries in the sterile sector of $M_\nu^{4\times4}$. The one zero textures of M_S are given by

$$M_S^1 = \begin{pmatrix} 0 & s_2 & s_3 \end{pmatrix}, M_S^2 = \begin{pmatrix} s_1 & 0 & s_3 \end{pmatrix}, M_S^3 = \begin{pmatrix} s_1 & 0 & s_3 \end{pmatrix} \tag{3}$$

The two-zero textures of $M_R^{4\times4}$ are achieved by mapping together the non-singular textures of M_R, one zero textures of M_S and all 81 textures of M_D. All the two-zero textures of $M_\nu^{4\times4}$ are given in Table 1.

Now the effective electron neutrino mass $|m_{ee}|$ and Jarlskog invariant J_{CP} has been studied for all the viable two-zero textures by following the given data in Table 2

Table 2: Best fit and 3σ values of active neutrino oscillation parameters [12] and current constraints on sterile neutrino parameters [11, 13, 14]. Here, $R_?$ is the solar to atmospheric mass squared difference ratio.

Parameter	Best Fit	3σ range
$\Delta m^2_{21}[10^{-5}eV^2]$	7.37	6.93-7.97
$\Delta m^3_{21}[10^{?3}eV^2]$(NH)	2.50	2.37-2.63
$\Delta m^3_{21}[10^{?3}eV^2]$(IH)	2.46	2.33-2.60
$\sin 2\theta_1 2/10^{?1}$	2.97	2.50-3.54
$\sin 2\theta_{13}/10[?2$(NH)	2.14	1.85-2.46
$\sin 2\theta_{13}/10^{?2}$(IH)	2.18	1.86-2.48
$\sin 2\theta_{23}/10^{?1}$(NH)	4.37	3.79-6.16
$\sin 2\theta_{23}/10^{?1}$(NH)	5.69	3.83-6.37
δ_{13}/π(NH)	1.35	0-2
δ_{13}/π(IH)	1.32	0-2
R_ν(NH)	0.0295	0.0263-0.0336
R_ν(IH)	0.0299	0.0266-0.0342
$\Delta m^2_{LSND}(\Delta m^2_{41})$ or $\Delta m^2_{43})eV^2$	1.63	0.87-2.04
$\lvert V_{e4}\rvert^2$	0.027	0.012-0.047
$\lvert V_{\nu 4}\rvert^2$	0.013	0.005-0.03
$\lvert V_{\tau 4}\rvert^2$	-	< 0.16

6. Viability of the two-zero textures under the study of neutrinoless double-beta decay and Jarlskog invariant with the current neutrino oscillation data:

We shall consider a texture to be viable under the study of neutrinoless double-beta decay if the value obtained from the plots of $|m_{ee}|$ shows consistency with current neutrino oscillation data and then calculate the range of J_{CP} for all the viable textures. We check the viability of the two-zero textures as follows. At first we calculate the ranges of $|m_{ee}|$ using the 3σ values of masses and mixing angles of the recent neutrino oscillation data (Table 2). We shall check the consistency of the two-zero textures under the study of neutrinoless double-beta decay by plotting against α by considering unconstrained and constrained Dirac and Majorana CP phases and similarly we will calculate J_{CP} by plotting it against δ_{13}. The plots are made for both the neutrino mass ordering i.e Normal hierarchy(NH) and Inverted hierarchy (IH). By constrained CP phases we mean that we pick up smaller ranges of values of unknown CP phases from complete range (0 - 2π). The textures are only considered to be viable if the value of $|m_{ee}|$ obtained from the plot are within the experimental range i.e the allowed value of $|m_{ee}|$ is within the range (0-0.1).Considering the parametrization of 4×4 PMNS lepton mixing matrix as [15, 16] we obtain the expressions of $|m_{ee}|$ and J_{cp} as given in equation (4),(5) and (6)

$$\langle m_{ee}\rangle_{(3+1)\nu} = \left|m_1 C_{12}^2 C_{13}^2 C_{14}^2 + m_2 S_{12}^2 C_{13}^2 C_{14}^2 e^{-i\alpha} + m_3 S_{13}^2 C_{14}^2 e^{-i\beta} + m_4 S_{14}^2 e^{-i\gamma}\right| \tag{4}$$

$$\langle m_{ee}\rangle_{(3+1)\nu} = \left|C_{14}^2 \langle m_{ee}\rangle_{3\nu} + S_{14}^2 \sqrt{\Delta m_{41}^2 e^{i\gamma}}\right| \tag{5}$$

$$J_{CP}^{4\nu} = C_{23}S_{23}S_{13}C_{24}^2C_{14}^2C_{13}^2C_{12}S_{12}sin\delta_{13} + S_{24}S_{14}C_{24}C_{23}C_{14}^2C_{13}^3C_{12}S_{12}sin(\delta_{14} - \delta_{24}) \tag{6}$$

6.1. Class A:

Texture A_1 and A_2 has ee=0, $e\mu$=0 and ee=0, $e\tau$=0, respectively in 4×4 form(Table 1). Since $|m_{ee}|$=0 in the A_1 and A_2 textures, therefore we donot get $|m_{ee}|$ plot for A_1 and A_2 textures. Therefore the texture is not viable under the study of neutrinoless double-beta decay. Now class A allows only NH spectrum in the 3+1 scenario. Therefore, we present only normal hierarchical case for class A.

On plotting J_{cp} with respect to δ_{13} with the CP phases running unconstrained from 0-2π , we see that the values of J_{CP} is in the range (0-0.05).

It was found that when we take constained CP phases i.e γ=δ_{13}=(0-30^0), β=δ_{24}=(0-45^0),δ_{14}=(180^0-225^0) and α=(315^0-360^0), texture A_1 and A_2 are viable[10]. When we plot J_{cp} vs δ_{13} we get the value of J_{cp}=(0-0.02). Figure 1 and Figure 2 shows the scatter plot of J_{cp} for the textures A_1 and A_2 for both unconstrained and constrained CP phases.

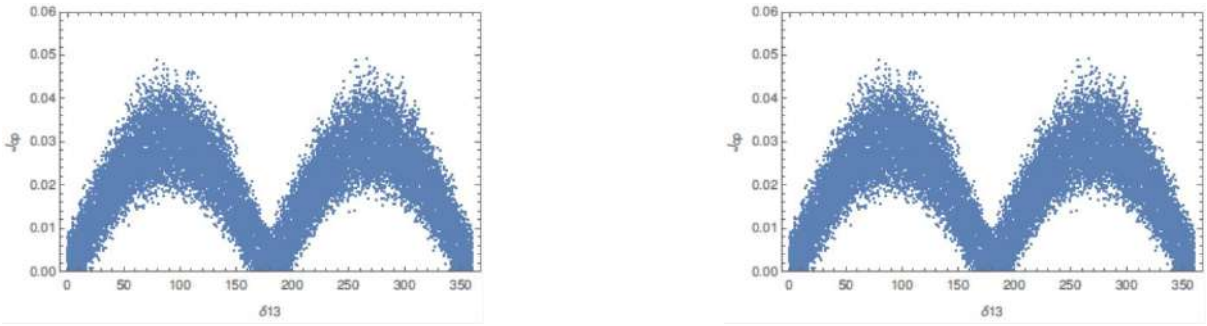

Figure 1: Scatter plots of J_{CP} against δ_{13}. The left and the right plot is for the unconstrained CP phases for the texures A_1 and A_2 respectively.

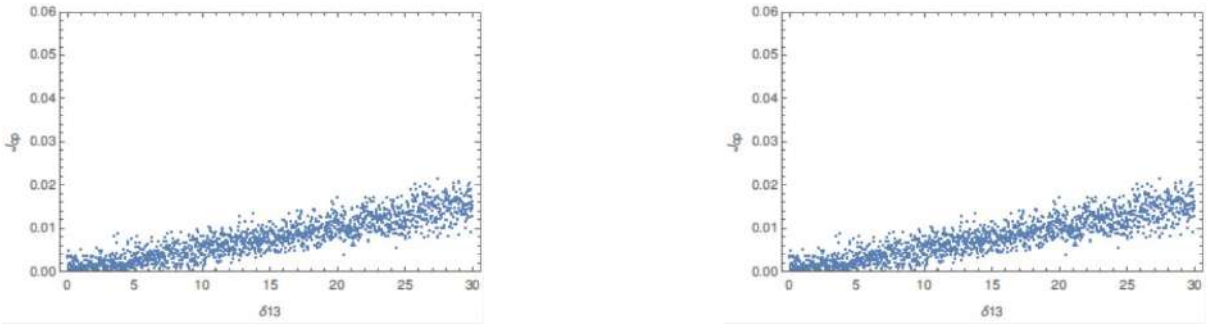

Figure 2: Scatter plots of J_{CP} against δ_{13}.Both left and the right plot is for the constrained CP phases(δ_{14}=(180^o-225^o), δ_{24}=(0-45^o), δ_{13}=(0-30^o))for the textures A_1 and A_2 respectively.

6.2. Class B:

Out of four textures B_1,B_2,B_3 and B_4 of class B, only B_3 and B_4 are of rank 3.In our study we will consider only the NH and IH spectrum of textures B_3 and B_4. $|m_{ee}|$ plots for B_3 and B_4 for unconstrained and constrained CP phases for NH spectrum are shown in the figure 3 and figure 4 respectively where the constrained ranges of CP phases are taken to be δ_{24}=α=(0-30^o), β=(180^o-225^o), δ_{13}=δ_{14}=γ=(0-45^o). Similary J_{CP} plots for both unconstrained and constrained CP phases for NH are shown in the figure 5 and figure 6 respectively. From figure 3 and figure 4 we have seen that texture B_3 and B_4 are viable under the study of neutrinoless double beta decay. On calculating J_{CP}, we get the range of J_{CP}=(0-0.05) for both the textures for unconstrained CP phases and J_{CP}=(0-0.03)for both the textures on considering constrained CP phases for NH spectrum.

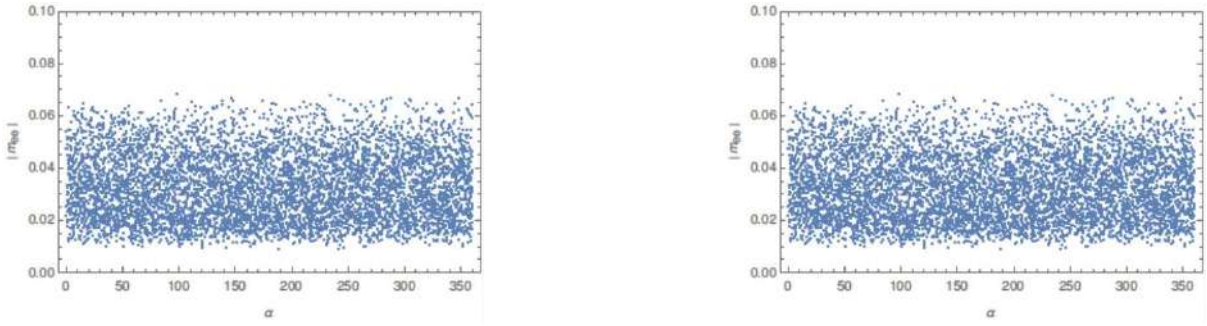

Figure 3: Scatter plots of $|m_{ee}|$ against α. The left and the right plot is for the unconstrained CP phases for the texures B_3 and B_4 respectively for NH spectrum.

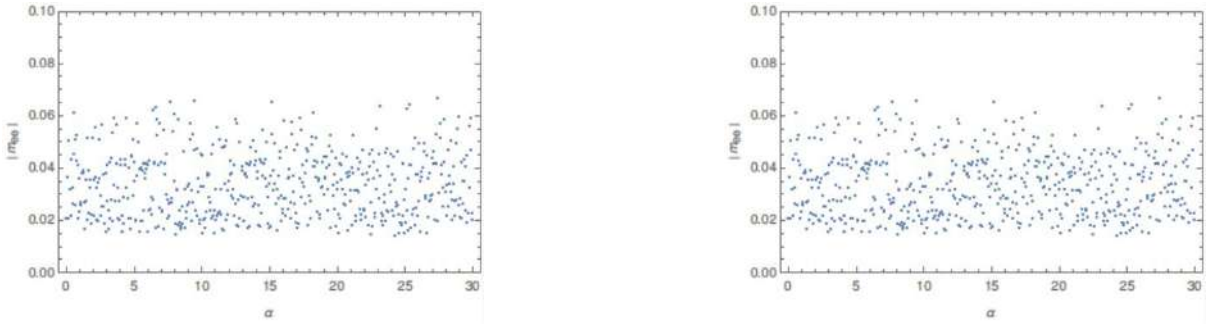

Figure 4: Scatter plots of $|m_{ee}|$ against α.The left plot and the right plot is for the textures B_3 and B_4 respectively for the constrained CP phases where the constrained ranges of CP phases are taken to be α=(0-30^o), β=(180^o-225^o), γ=(0-45^o) for NH spectrum.

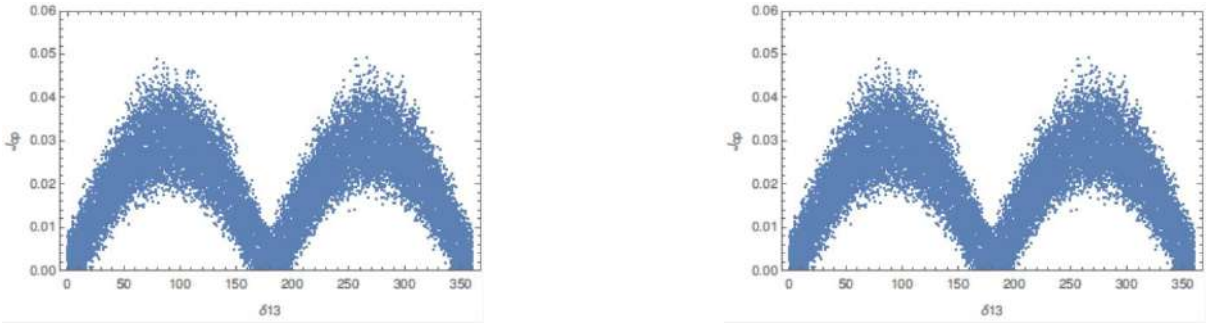

Figure 5: Scatter plots of J_{CP} against δ_{13}.Both left and the right plot is for unconstrained CP phases for the textures B_3 and B_4 respectively for NH spectrum.

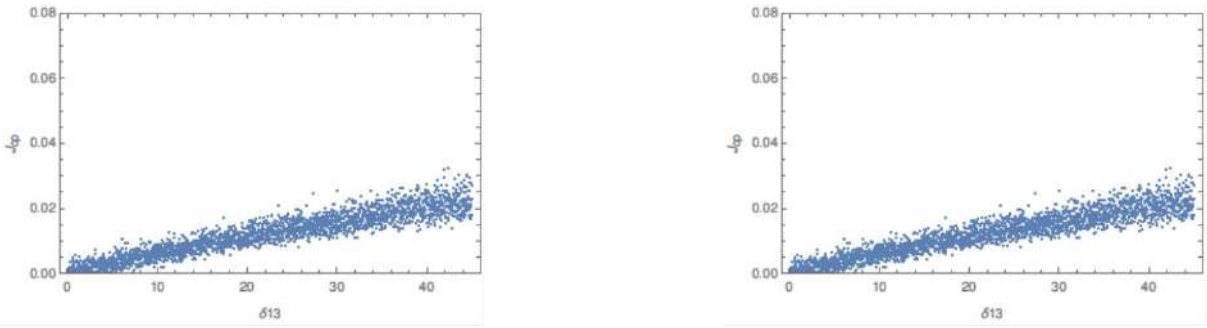

Figure 6: Scatter plots of J_{CP} against δ_{13}.The left plot and the right plot is for constrained CP phases(α=(0-30^o), β=(180^o-225^o), γ=(0-45^o) for the textures B_3 and B_4 respectively for NH.

Again we study the $|m_{ee}|$ plots for B_3 and B_4 for both unconstrained and constrained CP phases for IH spectrum, shown in figure 7 and figure 8. Similarly we calculate the J_{CP} plots for both constrained and unconstrained CP phases for IH, shown in figure 9.

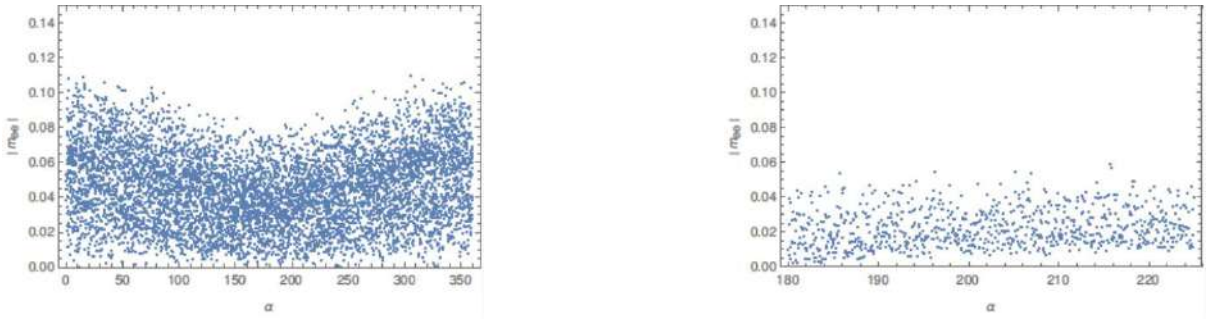

Figure 7: Scatter plots of $|m_{ee}|$ against α. The left and the right plot is for the unconstrained and constrained CP phases(γ=α=(180^o-225^o),β=(225^o-270^o)) respectively for the texture B_3 for IH spectrum.

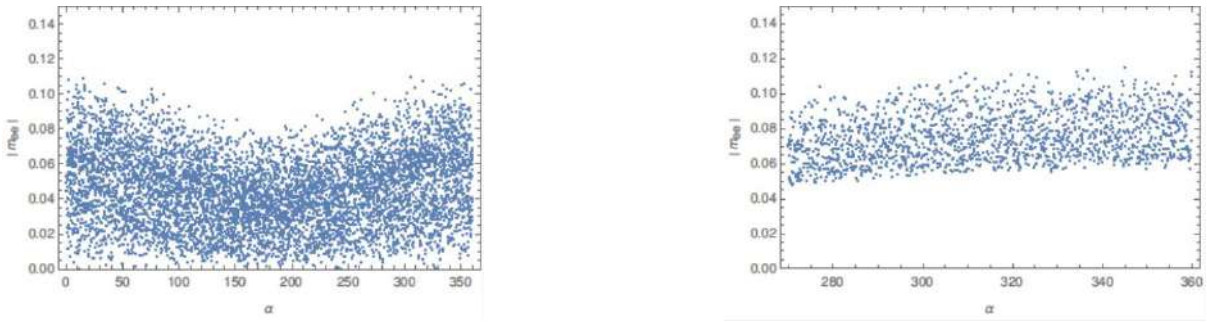

Figure 8: Scatter plots of $|m_{ee}|$ against α.The left and the right plot is for unconstrained and constrained CP phases(α=β=(315^o-360^o), γ=(270^o-360^o))respectively for the texture B_4 for IH spectrum.

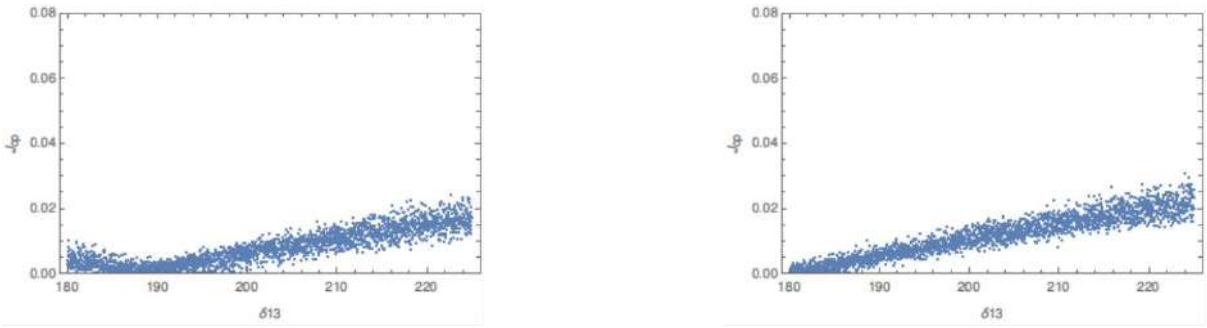

Figure 9: Scatter plots of J_{CP} against δ_{13}.The left plot is for the calculation of J_{CP} for texture B_3 when the CP phases are constrained within the range δ_{13}=(180^o-225^o),δ_{14}=(225^o-270^o),δ_{24}=(180^o-210^o) and the right plot is for texture B_4 when the CP phases are constrained within the range δ_{14}=δ_{24}=(0-30^o), δ_{13}=(180^o-225^o) for IH

For IH spectrum both texture B_3 and B_4 are viable under the study of neutrinoless double-beta decay.We get the value of J_{CP}=(0-0.05) for both the textures for unconstrained CP phases and J_{CP}=$(0-0.02)$ for both the textures for constrained CP phases.

6.3. Class C:

Class C consist of only one member, the class C itself. Here the scatter plots for $|m_{ee}|$ and J_{CP} for both NH and IH for both constrained and unconstrained CP phases are shown. Scatter plots for m_{ee} for NH and IH are shown for both constrained and unconstrained CP phases(δ_{24}=α=(0-30^o), β=(180^o-225^o),δ_{14}=δ_{13}=(0-45^o)δ_{13}=γ=(0-45^o)) in figure 10 and figure 11. Again the scatter plots of J_{CP} for NH are shown in figure 12.It is seen that texture C is viable under the study of neutrinoless double-beta decay for both constrained and unconstrained CP phases for both NH and IH spectrum. On calculating we get the range of J_{CP}=(0-0.05) for unconstrained CP phases for both NH and IH spectrum and J_{CP}=(0-0.02) and J_{CP}=(0-0.03)for constrained CP phases for NH and IH respectively.

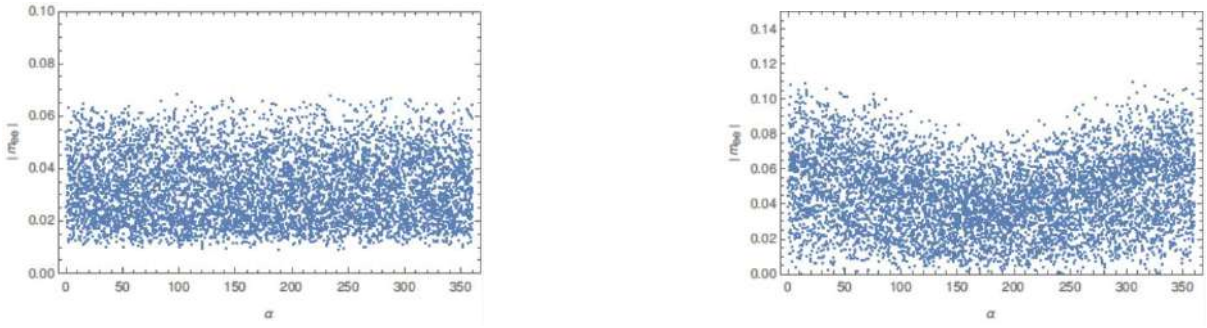

Figure 10: Scatter plots of $|m_{ee}|$ against α. The left and the right plot is for the unconstrained CP phases for the texture C for NH and IH spectrum respectively.

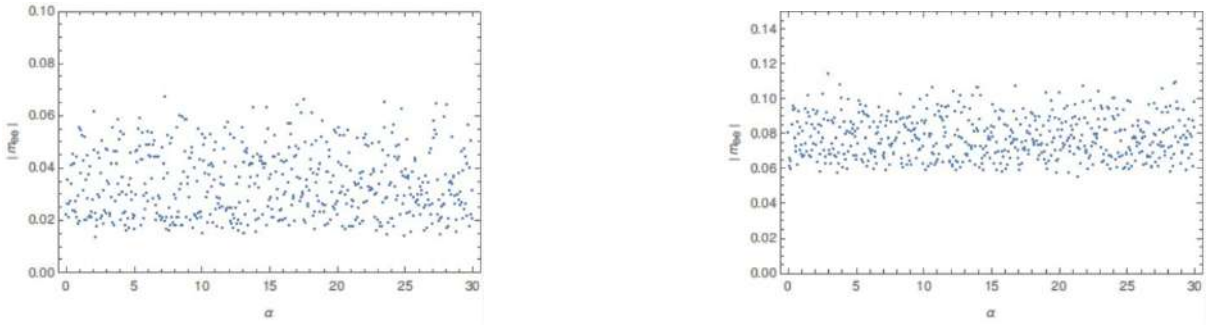

Figure 11: Scatter plots of $|m_{ee}|$ against α.Both left and the right plot is for the constrained CP phases: α=(0-30^o), β=(180^o-225^o), γ=(0-45^o)for the texture c for NH and IH spectrum respectively.

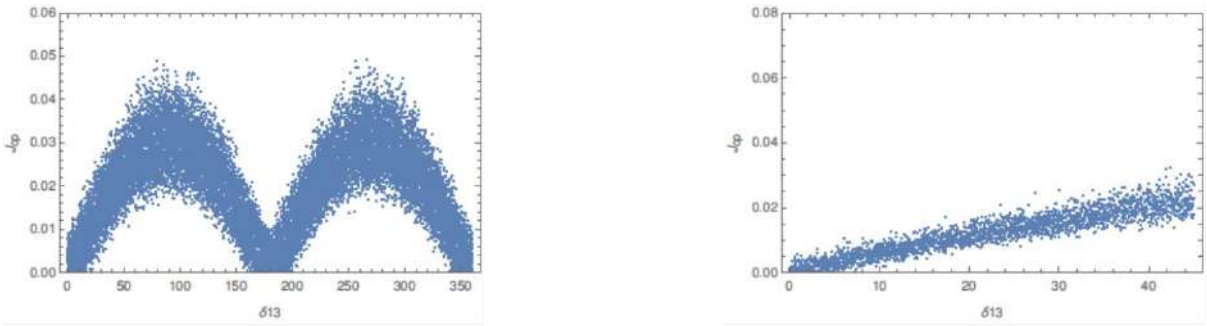

Figure 12: Scatter plots of J_{CP} against δ_{13}. The left and the right plot is for unconstrained CP phases and constrained CP phases (δ_{14}=δ_{13}=(0-45^o),δ_{24}=(0-45^o))for NH respectively.

6.4. Class D:

The class D consist of two textures D_1 and D_2. Both NH and IH are favoured by these two textures. The $|m_{ee}|$ plots for NH for unconstrained CP phases and constrained CP phases for the texture D_1 are shown in figure 13 where the range of constrained CP phases are taken to be γ=δ_{13}=(0-30^0), β=δ_{24}=(0-45^0),δ_{14}=(180^0-225^0) and α=(315^0-360^0).For IH spectrum texture D_1 is allowed for unconstrained CP phases and when the CP phases are constrained to γ=δ_{24}=(0-10^o), δ_{13}=δ_{14}=(0-30^o),α=(0-20^o),β=unconstrained,the texture is forbidden under the study of neutrinoless double-beta decay.For both NH and IH spectrum, texture D_2 is forbidden for unconstrained CP phases as well as for constrained CP phases. Again J_{CP} is calculated for NH spectrum for texture D_1 are shown in figure 14.

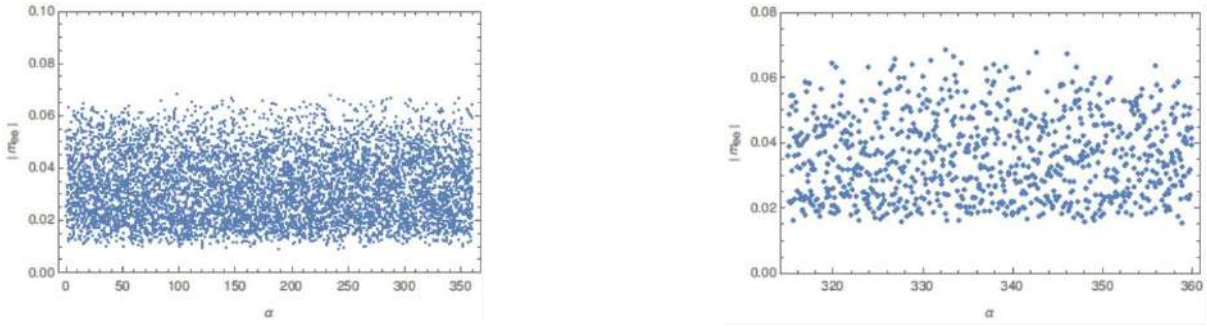

Figure 13: Scatter plots of $|m_{ee}|$ against α. The left and the right plot is for unconstrained CP phases and constrained CP phases respectively where the ranges of constrained CP phases are taken to be α=(315^o-360^o), β=(0-45^o), γ=(0-30^o)for the texture D_1 for NH spectrum.

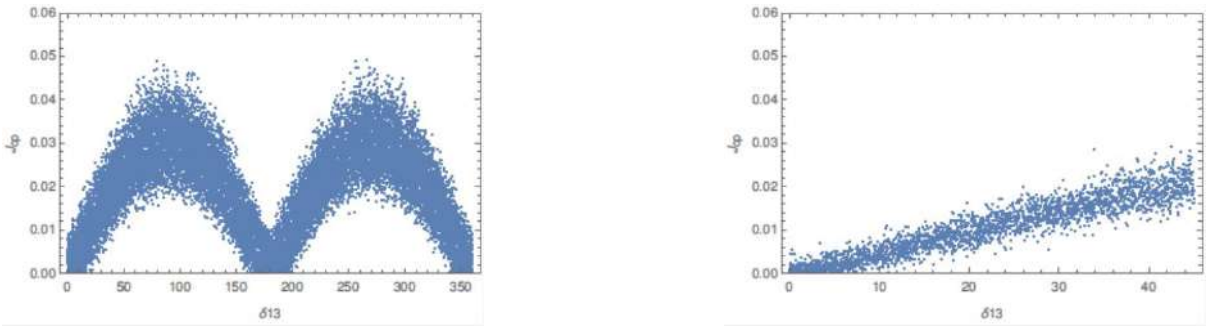

Figure 14: Scatter plots of J_{CP} against δ_{13}. The left and the right plot is for the unconstrained and constrained CP phases respectively for the texture D_1 where the range of constrained CP phases are taken to be δ_{13}=δ_{24}=(0-45^o),δ_{14}=(0-30^o) for NH spectrum.

It is seen that for texture D_1 the value of J_{CP} is within the range (0-0.05) for unconstrained CP phases and J_{CP}=(0-0.03) for constrained CP phases for NH spectrum.Texture D_1 is viable under the study of neutrinoless double beta decay for NH spectrum.

6.5. Class E:

Class E consist of two textures E_1 and E_2. Texture E_1 and E_2 as they show very poor overlapping on plotting the correlation obtained in the paper [10]. Both the textures are ruled out.

6.5. Class F:

Class F consist of three textures F_1, F_2 and F_3. In MES mechanism the textures are restricted to only NH and IH spectrum. Texture F_1: We study the $|m_{ee}|$ scatter plots for texture F_1 for unconstrained CP phases and for constrained CP phases where we take the constrained ranges of CP phases to be (γ=δ_{24}=(130^o-180^o),δ_{14}=β=δ_{13}=α=(0-30^o)) for NH spectrum shown in figure 15. From figure 16 we also calculate J_{CP} for both unconstrained and constrained CP phases for NH.

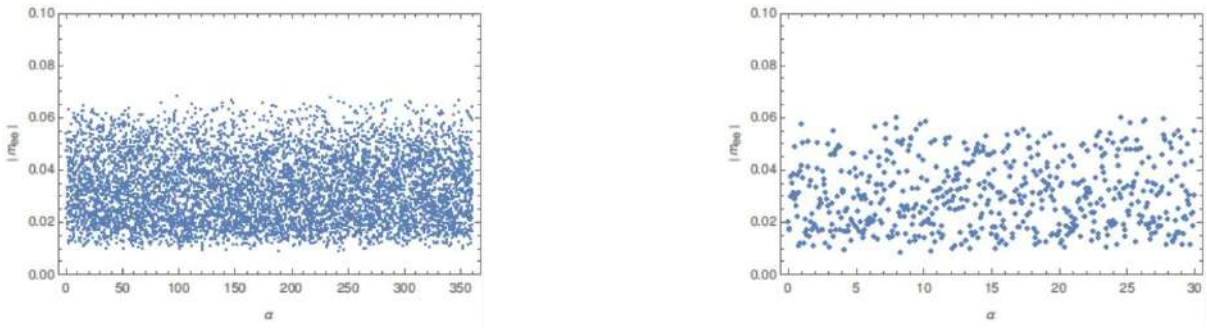

Figure 15: Scatter plots of $|m_{ee}|$ against α. The left and the right plot is for the unconstrained and constrained CP phases respectively for the texture F_1 where the range of constrained CP phases are taken to be β=α=(0-30^o),γ=(130^o-180^o) for NH.

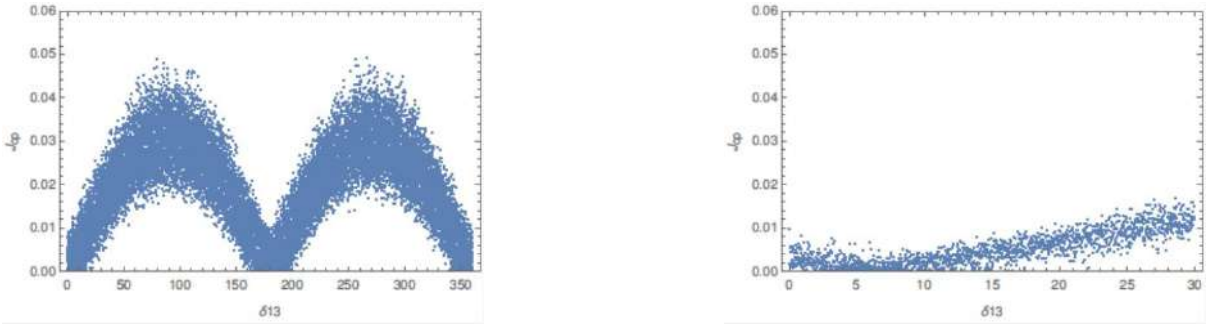

Figure 16: Scatter plots of J_{CP} against δ_{13}. The left and the right plot is for the unconstrained and constrained CP phases respectively for the texture F_1 where the range of constrained CP phases are taken to be δ_{13}=δ_{24}=(0-30^o),δ_{14}=(130^o-180^o) for NH.

Again in case of IH spectrum, in figure17 we have shown the $|m_{ee}|$ scatter plots for unconstrained and constrained CP phases, here the constrained ranges of CP phases are taken to be γ=(210^o-225^o),δ_{14}=(0-30^o),β=(120^o-150^o),δ_{13}=(140^o-180^o),α=δ_{24}=(340^o-360^o).We also calculate J_{CP} for unconstrained CP phases and the specified ranges of constrained CP phases shown in figure18.

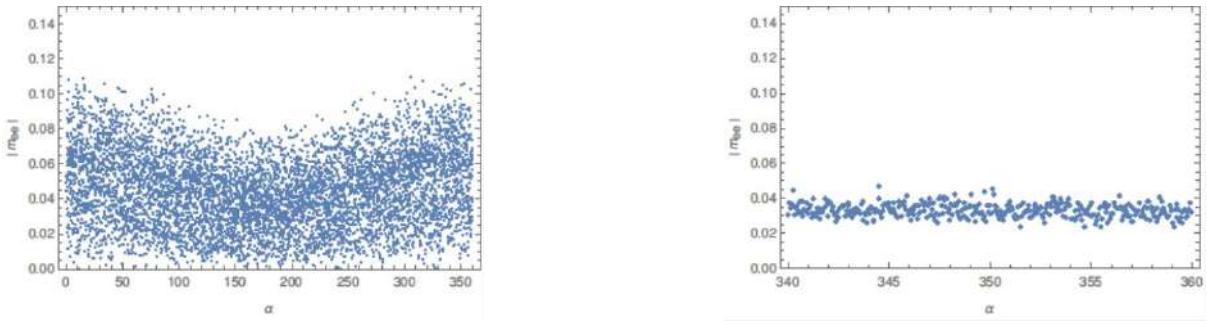

Figure 17: Scatter plots of $|m_{ee}|$ against α. The left and the right plot is for the unconstrained and constrained CP phases respectively for the texture F_1 where the range of constrained CP phases are taken to be β=(120^o-150^o),α=(340^o-360^o),γ=(210^o-225^o) for IH.

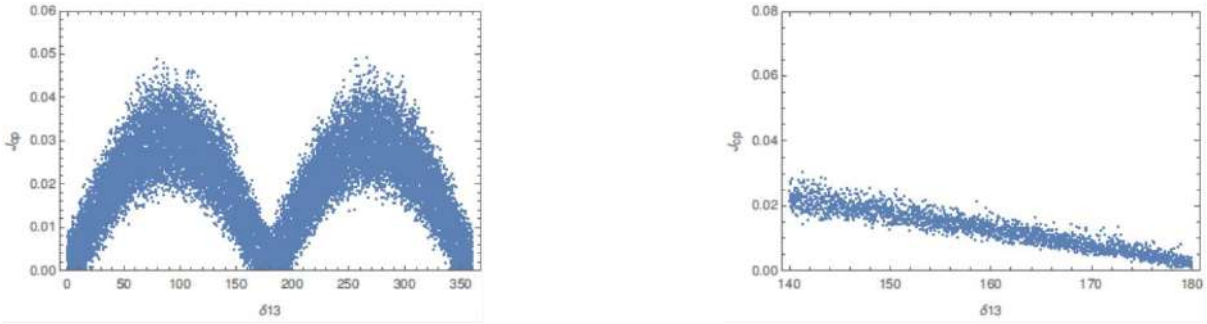

Figure 18: Scatter plots of J_{CP} against δ_{13}. The left and the right plot is for the unconstrained and constrained CP phases respectively for the texture F_1 where the range of constrained CP phases are taken to be δ_{13}=(140^o-180^o),δ_{24}=(340^o-360^o),δ_{14}=(0-30^o) for IH.

Texture F_2: We study the $|m_{ee}|$ scatter plots for texture F_2 for unconstrained CP phases and constrained CP phases where we take the constrained ranges of CP phases to be (γ=(315^o-360^o),δ_{14}=(0-30^o),β=(270^o-315^o),δ_{13}=(120^o-180^o),α=(0-45^o),δ_{24}=(0-360^o)) for NH spectrum shown in figure 19. In figure 20 we also calculate J_{CP} for both unconstrained and constrained CP phases for NH.

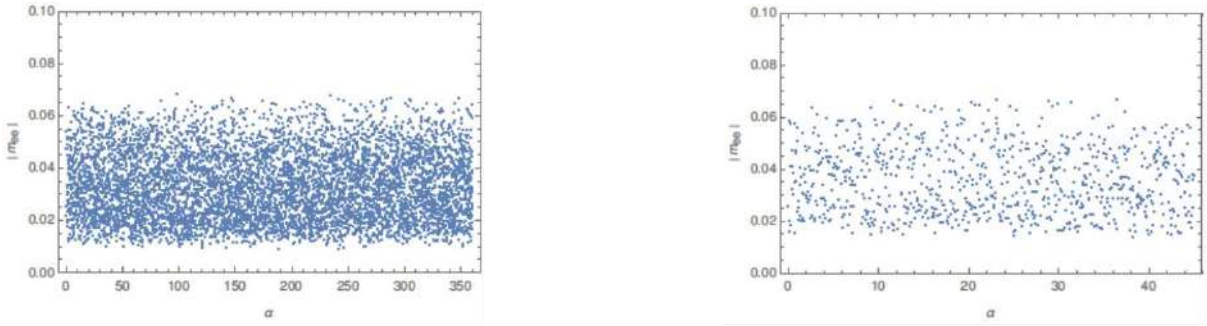

Figure 19: Scatter plots of $|m_{ee}|$ against α. The left and the right plot is for the unconstrained and constrained CP phases respectively for the texture F_2 where the range of constrained CP phases are taken to be β=(270^o-315^o),α=(0-45^o),γ=(315^o-360^o) for NH.

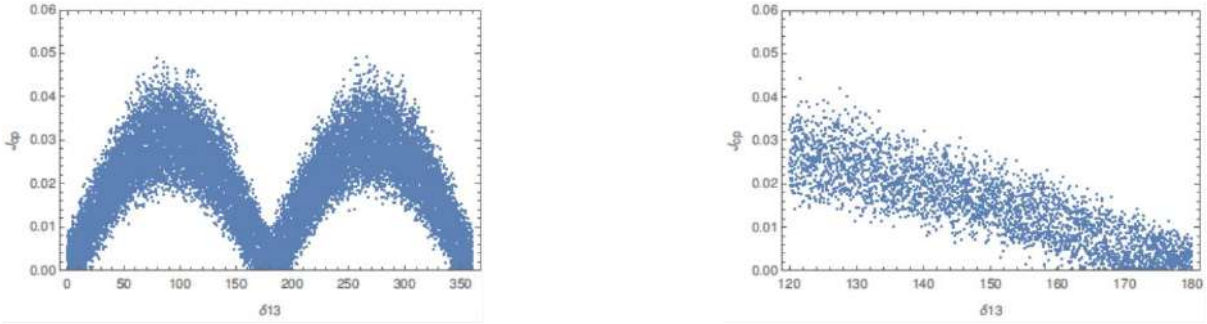

Figure 20: Scatter plots of J_{CP} against δ_{13}. The left and the right plot is for the unconstrained and constrained CP phases respectively for the texture F_1 where the range of constrained CP phases are taken to be δ_{13}=(120^o-180^o),δ_{24}=(0-360^o),δ_{14}=(0-30^o) for NH.

Now we study the $|m_{ee}|$ scatter plots in case of IH spectrum for texture F_2 for both unconstrained and constrained CP phases.Here we take the range for constrained CP phases to be γ=(0-100^o), δ_{14}=(0-30^o), α=(0-60^o), δ_{13} = δ_{24} = β = unconstrained. $|m_{ee}|$ plots are shown in figure 21. Similarly we calculated J_{CP} for constrained and unconstrained CP phases.

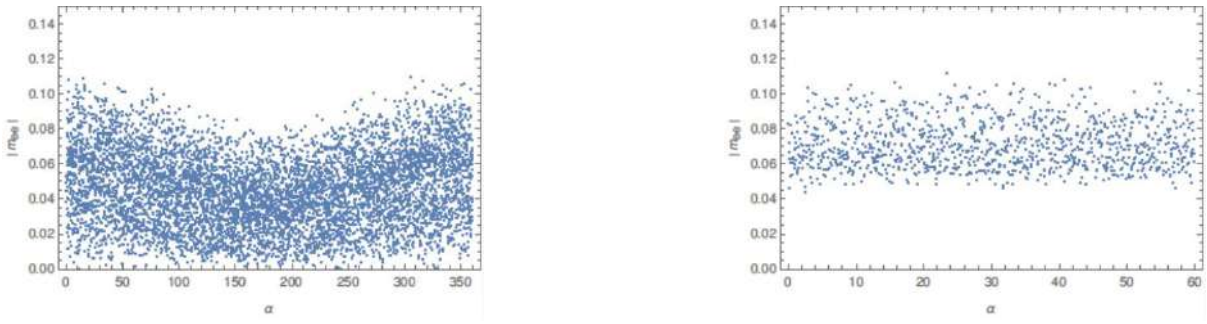

Figure 21: Scatter plots of $|m_{ee}|$ against α. The left and the right plot is for the unconstrained and constrained CP phases respectively for the texture F_2 where the range of constrained CP phases are taken to be β=unconstrained,α=(0-60^o),γ=(0-100^o) for IH.

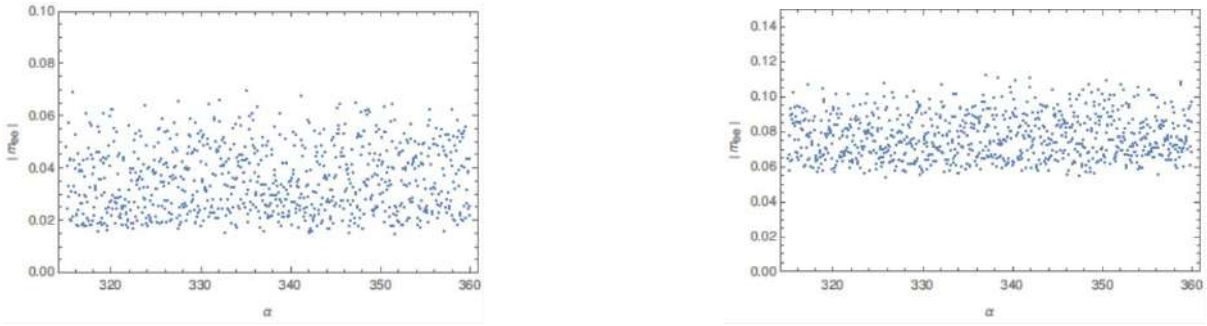

Figure 22: Scatter plots of $|m_{ee}|$ against α. The left and the right plot is for NH and IH spectrum respectively for constrained CP phases for the texture F_3 where the range of constrained CP phases are taken to be β=(0-45^0),α=(315^0-360^o),γ=(0-30^o).

Table 3: Ranges of $|m_{ee}|$ and J_{CP} obtained for the different two-zero textures are given in the table. Textures which are not allowed are lebelled as NA.

Texture	Range of $\|m_{ee}\|$				Range of J_{CP}			
	unconstrained cp phases		constrained cp phases		unconstrained cp phases		constrained cp phases	
	NH	IH	NH	IH	NH	IH	NH	IH
A_1	NA	-	NA	-	0-0.05	-	0-0.02	-
A_2	NA	-	NA	-	0-0.05	-	0-0.02	-
B_3	0.01-0.06	0-0.1	0.02-0.06	0-0.04	0-0.05	0-0.05	0-0.02	0-0.02
B_4	0.01-0.06	0-0.1	0.015-0.06	0.05-0.1	0-0.05	0-0.05	0-0.02	0-0.02
C	0.01-0.06	0-0.1	0.02-0.06	0.06-0.1	0-0.05	0-0.05	0-0.02	0-0.03
D_1	0.01-0.06	0-0.1	0.02-0.07	NA	0-0.05	0-0.05	0-0.03	NA
D_2	NA	NA	NA	NA	-	-	-	-
E_1	-	-	-	-	-	-	-	-
E_2	-	-	-	-	-	-	-	-
F_1	0.01-0.06	0-0.1	0.01-0.06	0.03-0.04	0-0.05	0-0.05	0-0.02	0-0.02
F_2	0.01-0.06	0-0.1	0.02-0.06	0.06-0.1	0-0.05	0-0.05	0-0.03	0-0.02
F_3	0.01-0.06	0-0.1	0.02-0.06	0.06-0.1	0-0.05	0-0.05	0-0.02	0-0.03

We have seen that texture F_2 is viable under under the study of neutrinoless double beta decay under the IH scheme when the CP phases are constrained to the range β=α=(120^o-150^o),γ=(210^o-225^o). Similarly texture F_3 is also viable under the study of neutrinoless double beta decay for both unconstrained and constrained CP phases for NH and IH spectrum. The $|mee|$ plot for texture F_3 for unconstrained CP phases is same as fig 10 and plot for the constrained CP phases(γ=δ_{13}=(0-30^0), β=δ_{24}=(0-45^0),δ_{14}=(180^0-225^0) and α=(315^0-360^0)) for both NH and IH spectrum are shown in fig 22. We have also calculated J_{CP} for for texture F_3.

Finally we have presented the range of $|m_{ee}|$ and J_{CP} of all the two zero textures in Table 3.

7. Conclusion:

In our analysis we have found that for all the textures $|m_{ee}|$ lies within the experimental constraints. We have presented the scatter plots of $|m_{ee}|$ for all the textures except A_1, A_2 for which $|m_{ee}| = 0$, texture D_2, E_1, E_2 which are not allowed by experimental constraints in the context of MES mechanism. We have also calculated J_{CP} for the viable two zero textures. On calculating J_{CP} for all the textures we have seen that $J_{CP} \leq 0.05$ and the peaks depend on δ_{14} and δ_{24}. When δ_{14}=δ_{24} then both the peaks are equal. Unlike the three neutrino scenario whereby $J_{CP} = 0$ for $\delta_{13} = 0$, in (3+1) scheme $J_{CP} \neq 0$ even when $\delta_{13} = 0$.

References:

[1] C. Athanassopoulos, L. Auerbach, R. Burman, I. Cohen, D. Caldwell, B. Dieterle, J. Donahue, A. Eisner, A. Fazely, F. Federspiel, et al., "Evidence for $\nu\ \mu \rightarrow \nu$ e Oscillations from the LSND Experiment at the Los Alamos Meson Physics Facility," Physical Review Letters, vol. 77, no. 15, p. 3082, 1996.
[2] A. Aguilar-Arevalo, B. Brown, L. Bugel, G. Cheng, E. Church, J. Conrad, R. Dharmapalan, Z. Djurcic, D. Finley, R. Ford, et al., "Improved search for $\nu\ \mu \rightarrow \nu$ e oscillations in the MiniBooNE experiment," Physical review letters, vol. 110, no. 16, p. 161801, 2013.
[3] M. A. Acero, C. Giunti, and M. Laveder, "Limits on ν e and ν e disappearance from Gallium and reactor experiments," Physical Review D, vol. 78, no. 7, p. 073009, 2008.
[4] C. Giunti and M. Laveder, "Statistical significance of the gallium anomaly," Physical Review C, vol. 83, no. 6, p. 065504, 2011.
[5] G. Mention, M. Fechner, T. Lasserre, T. A. Mueller, D. Lhuillier, M. Cribier, and A. Letourneau, "Reactor antineutrino anomaly," Physical Review D, vol. 83, no. 7, p. 073006, 2011.
[6] J. Gomez-Cadenas and M. C. González-Garciá, "Futurev τ oscillation experiments and present data," Zeitschrift für Physik C Particles and Fields, vol. 71, no. 1, pp. 443-454, 1996.
[7] S. Goswami, "Accelerator, reactor, solar, and atmospheric neutrino oscillations: Beyond three generations," Physical Review D, vol. 55, no. 5, p. 2931, 1997.
[8] J. Barry, W. Rodejohann, and H. Zhang, "Light sterile neutrinos: models and phenomenology," Journal of High Energy Physics, vol. 2011, no. 7, p. 91, 2011.
[9] J. Heeck and H. Zhang, "Exotic charges, multicomponent dark matter and light sterile neutrinos," Journal of High Energy Physics, vol. 2013, no. 5, p. 164, 2013.
[10] M. Patgiri and P. Kumar, "Understanding of two-zero textures of neutrino mass matrices in minimal extended seesaw mechanism and their symmetry realization," International Journal of Modern Physics A, vol. 34, no. 11, p. 1950059, 2019.
[11] M. Ghosh, S. Goswami, and S. Gupta, "Two-zero mass matrices and sterile neutrinos," Journal of High Energy Physics, vol. 2013, no. 4, p. 103, 2013.
[12] F. Capozzi, E. Lisi, A. Marrone, D. Montanino, and A. Palazzo, "Neutrino masses and mixings: Status of known and unknown 3ν parameters," Nuclear Physics B, vol. 908, pp. 218-234, 2016.
[13] S. Gariazzo, C. Giunti, M. Laveder, Y. Li, and E. Zavanin, "Light sterile neutrinos," Journal of Physics G: Nuclear and Particle Physics, vol. 43, no. 3, p. 033001, 2016.
[14] C. Giunti, "Oscillations beyond three-neutrino mixing," arXiv preprint arXiv:1609.04688, 2016.
[15] S. Goswami and W. Rodejohann, "Constraining mass spectra with sterile neutrinos from neutrinoless double beta decay, tritium beta decay, and cosmology," Physical Review D, vol. 73, no. 11, p. 113003, 2006.
[16] P. Kumar and M. Patgiri, "Minimal extended seesaw and group symmetry realization of two-zero textures of neutrino mass matrices," Nuclear Physics B, p. 115082, 2020.